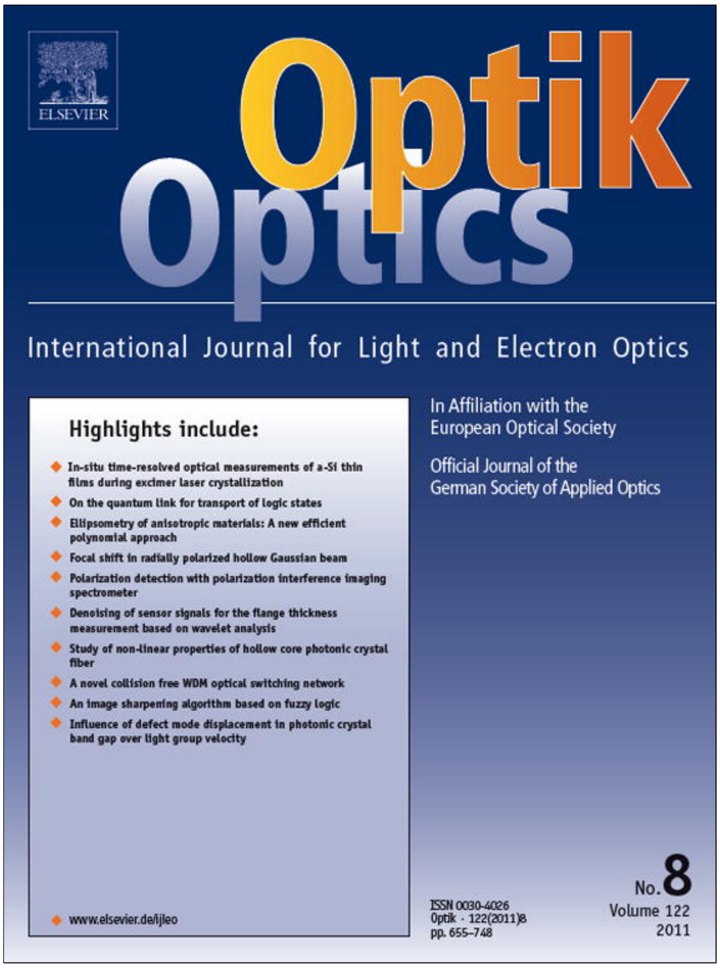
ELSEVIER
Optik
Optics
International Journal for Light and Electron Optics
Highlights include:
In-situ time-resolved optical measurements of a-Si thin films during excimer laser crystallization
On the quantum link for transport of logic states
Ellipsometry of anisotropic materials: A new efficient polynomial approach
Focal shift in radially polarized hollow Gaussian beam
Polarization detection with polarization interference imaging spectrometer
Denoising of sensor signals for the flange thickness measurement based on wavelet analysis
Study of non-linear properties of hollow core photonic crystal fiber
A novel collision free WDM optical switching network
An image sharpening algorithm based on fuzzy logic
Influence of defect mode displacement in photonic crystal band gap over light group velocity
www.elsevier.de/ijleo
In Affiliation with the European Optical Society
Official Journal of the German Society of Applied Optics
ISSN 0030-4026
Optik · 122(2011)8
pp. 655–748
No. 8
Volume 122
2011

Optik 122 (2011) 681–686

Contents lists available at ScienceDirect

Optik

journal homepage: www.elsevier.de/ijleo

Denoising of sensor signals for the flange thickness measurement based on wavelet analysis

Zhifeng Zhang [a,*], Zhan Su [b], Yuling Su [a], Zhan Gao [c]

[a] Zhengzhou University of Light Industry, Department of Physics, Zhengzhou 450002, China
[b] Henan Automation Engineering and Technology Research Center, Zhengzhou 450008, China
[c] Key Laboratory of Luminescence and Optical Information, Beijing Jiaotong University, Ministry of Education, Beijing 100044, China

ARTICLE INFO

Article history:
Received 3 September 2009
Accepted 6 May 2010

Keywords:
Flange thickness
Wheelset
Denoising
Laser displacement sensor
FFT

ABSTRACT

A railway wheelset is subject to normal wear due to large part to friction contact between the wheelset and the rail. Because the wear of wheelset will bring the hidden security troubles to the operation of the railway, it is very important to measure the wheelset's geometrical parameters, especially the flange thickness. The optoelectronic method is proposed and can dynamically measure the flange thickness on line. Fast Fourier transform and wavelet analysis methods are used to denoise the sensor's signals. It is found that the wavelet transform produces a much better way of denoising of the signals compared with the fast Fourier transform. Comparisons of the flange thickness measurement with the wheelset creeping and the optoelectronic system are presented. The root-mean-square errors of the flange thickness with the manual measurement with the wheelset creeping and the optoelectronic method measurement with the wavelet analysis are 0.22 and 0.18, respectively. The changing range of manual measurement is much larger than that of the optoelectronic method because of the difference between every operator's measuring standard. Measurement results of the optoelectronic method show that the system has better repeatability and reliability compared to the manual measurement.

1. Introduction

A railway wheelset is subject to normal wear due in large part to friction contact between the wheelset and the rail [1]. As a railway wheelset wears, the profile of the running surface and many critical dimensions of the wheelset change due to dynamic interaction of the wheelset with the rail. The flange thickness is a key parameter that influences the wheel–rail contact. The change of the flange thickness will certainly bring hidden security troubles to the operation of railway, so it is very important to measure the geometric parameters of the wheelset [2].

The measuring methods and systems have been researched in recent years [3–10]. However, safety check measurements of the wheelsets mostly still take place in train yards. All the wheelsets are visually inspected and only a wheelset with noticeable wear can be measured. Many technicians usually spend long times on the safety check of wheelsets and most of the measurements are still depend on the special mechanic tools by manual work, especially in China, so there is often big difference of the measurement results to the flange thickness between different operators. It is very important to realize dynamic and real-time measurements of the wheelset's geometric parameters [11–13].

One of the standard methods to remove the noise of the signal is the fast Fourier transform (FFT) which is the linear Fourier smoothing. Wavelet theory has been developed strongly in the past 10 years and been applied in various research fields: the quality improvement of signals or images [14], and data mining in a limited number of images [15], and real-time 3D cardiac ultrasound [16], and analysis of electrocardiograms [17], and neuroscience [18] and noise reduction in astronomical spectra [19,20], and texture synthesis and modeling [21]. The wavelet method can obtain better results in the analysis of non-stationary or non-periodical signals than FFT. In general, the measuring practical data of the optoelectronic sensors detecting are contaminated by the noise, so the noise removal is important to get the higher measurement accuracy. In this paper, FFT filter and wavelet analysis are used to denoise the practical data. The results obtained with two methods show that the wavelet method is prior to FFT in the noise removal of the practical data.

* Corresponding author.
E-mail address: zhifengzhang76@gmail.com (Z. Zhang).

0030-4026/$ – see front matter © 2010 Elsevier GmbH. All rights reserved.
doi:10.1016/j.ijleo.2010.05.006

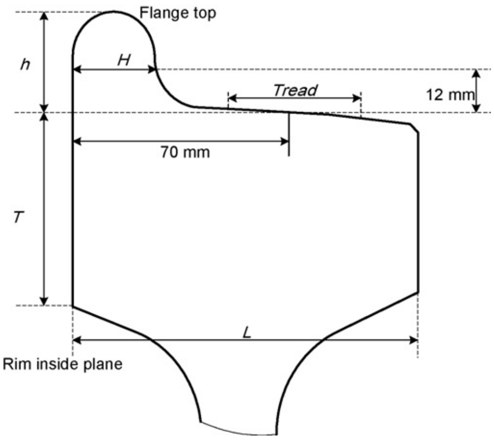

Fig. 1. Profile of wheelset section.

2. Measuring principle

2.1. *Definition of wheelset's parameters*

Fig. 1 shows the profile of the part wheelset. Tread is the contacting zone with the rail when the wheelset moves. There is a base point on the tread and the distance is 70 mm to rim inside plane. Flange base line is the horizontal line 12 mm above the contacting point of the wheelset and rail. Flange height *h* is the height between flange base line and flange top. Flange thickness *H* is the horizontal thickness along flange base line. After the wheelset worked a long time, the flange height and thickness will change which is called the flange wear. Rim thickness *T* is the distance between the flange base line to the bottom of rim inside plane. Rim width *L* is the distance between rim inside base plane and the outside base plane. These parameters belong to geometric parameters of wheelset.

Fig. 2 shows the sketch diagram flange wearing. After wheel working a long time, the flange will turn thin, or sharp, or orthogonal. The flange thickness will change which is very dangerous. The optoelectronic system proposed can measure the change of this parameter on line. When the wheelsets pass through the measurement system, the measurement results of flange thickness are obtained. When the results of some wheelsets are beyond the limitation, the system will alarm and the technicians can repair or replace these wheelsets correctly and duly. This measurement system also can be combined with other measurement instruments to assess the wheelsets qualities.

2.2. *Measuring principle and system*

The optoelectronic system based on the laser displacement sensor can measure the flange thickness. The laser displacement sensor is composed of two sub-systems: one is the optical emitting system which uses a semiconductor laser with the wavelength 635 nm and light power 5 mW (THORLABS HL6312G) and the other is the optical receiving system which uses the linear CCD detector (NEC UPD3753). Fig. 3 shows the calibration result of the laser displacement sensor with a grating ruler (LG-50). The measurement range of the laser displacement sensor is 110 ± 15 mm. The response frequency of the laser displacement is 400 Hz. The laser sensor

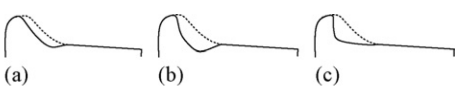

Fig. 2. Sketch diagram of different flange wearing. (a) Thin after wearing, (b) sharp after wearing and (c) orthogonal after wearing.

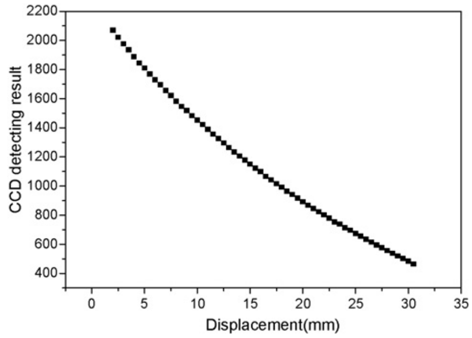

Fig. 3. The laser sensor calibration curve.

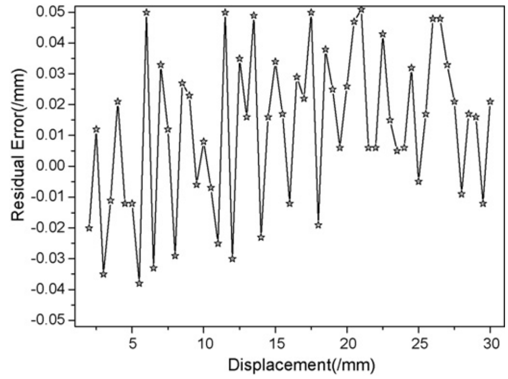

Fig. 4. The residual errors vs displacement curve.

resolution is 0.02 mm. Fig. 4 shows the relation of the residual error and the displacement. The maximum residual error is 0.05 mm.

Fig. 5 shows the measuring principle and the measuring system. Fig. 5(a) shows the cross-section diagram of the system and Fig. 5(b) shows the top-view diagram. Measurement system fixed on the connection place of two rails is composed of two laser displacement sensors, laser sensor 1 and laser sensor 2. There is about ten centimeters gap between two rails in China, so the light emitted by laser sensor 1 can be projected on the wheel's point under the rail 12 mm according to the definition of flange thickness when the wheel passes through. Light emitted by laser sensor 2 is projected on the rim inner plane. Fig. 6 shows the schematic diagram of the measuring system on the scene. The flange thickness of the wheel can be obtained from Eq. (1):

$$H = L_0 - (L_1 + L_2) \tag{1}$$

where H is the flange thickness of wheel; L_0 is the distance between laser sensor 1 and laser sensor 2; L_1, and L_2 are the measuring results of laser sensor 1 and laser sensor 2, respectively.

3. Denoising algorithms

3.1. *Fast Fourier transform denoising algorithm*

For the signal $f(t)$, the Fourier transform $\hat{f}(\omega)$ can be obtained by the inner product of $f(t)$ with a sinusoidal wave $e^{i\omega t}$ according to Eq. (2):

$$\hat{f}(\omega) = \left\langle f(t), e^{i\omega t} \right\rangle = \int_{-\infty}^{\infty} f(t) e^{i\omega t} dt \tag{2}$$

It transforms the signal $f(t)$ from the time domain to the frequency domain ω and is viewed as the basis of modern signal processing. FFT [22] is the standard method for observing signals in the frequency domain. By suppressing the high-frequency com-

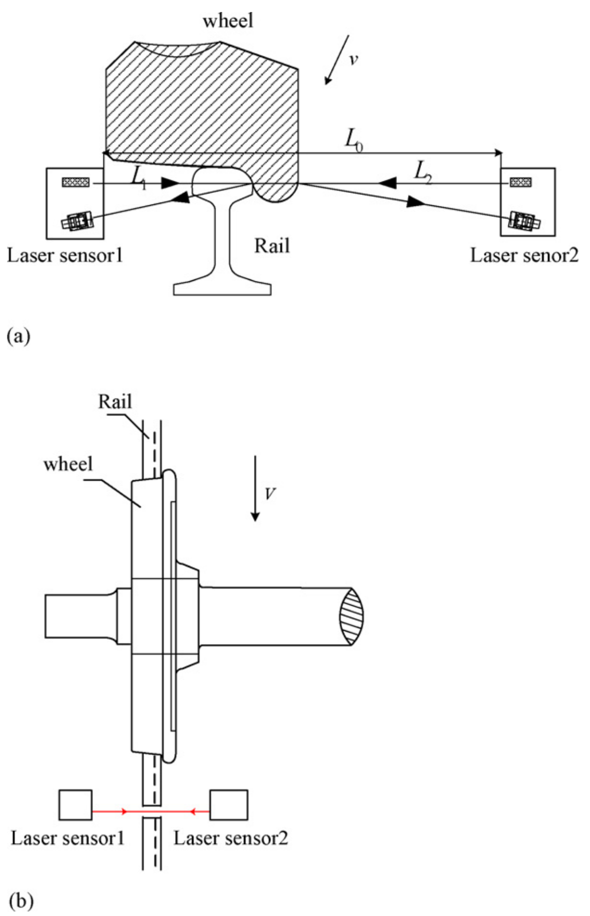

Fig. 5. Scheme diagram of measurement system: (a) the cross-section diagram of the system: (b) the top-view diagram of the system.

ponents, the noise of the signal can be removed. It works as a perfect low-pass filter by cutting off frequency during the signal analysis. In spite of its earlier popularity, Fourier transform has certain serious theoretical limitation in processing signals. Eq. (2) showed that $\hat{f}(\omega)$ is the integration of $f(t)$ for all times $t\in(-\infty, +\infty)$ and this makes it difficult to analyze any local property of $f(t)$ from $\hat{f}(\omega)$.

3.2. Wavelet denoising algorithm

Wavelet analysis is a new time-frequency analysis method without the constraint of periodicity or infinite time in the sampled signals. In the low-frequency part, one can get the high frequency and low time resolutions; in contrast in the high-frequency part,

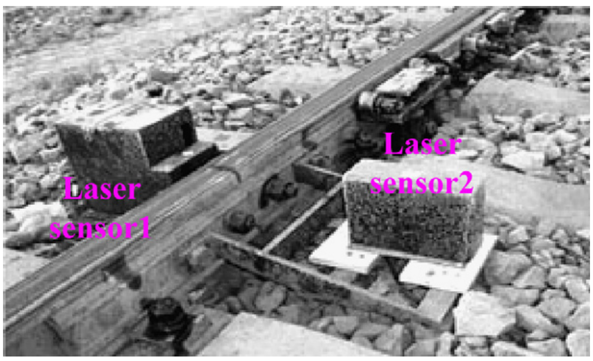

Fig. 6. schematic diagram of the measuring system on the scene.

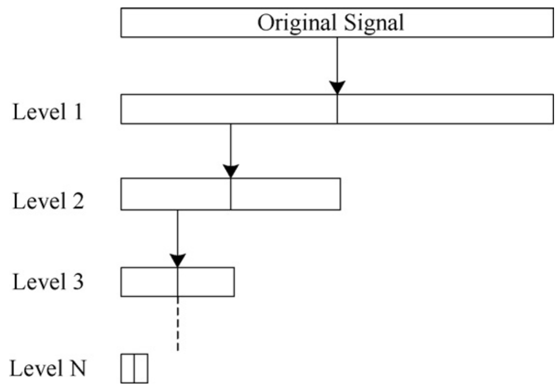

Fig. 7. Scheme of fast discrete wavelet transform. The symbol a_j indicates the approximation coefficient from a low-pass filter and d_j is a detail coefficient from the high-pass filter at level j (j = 1, 2, 3 . . . N).

low frequency and high time resolutions are obtained [23]. Fig. 7 showed the principle of wavelet analysis. An original signal is decomposed to a high- and low-frequency component at several decomposition levels:

$$f_{j,t} = \sum_{m=1}^{M} h_m S_{j-1,((2j-m) \bmod N/2^{j-1})+1} \quad (3)$$

$$F_{j,t} = \sum_{m=1}^{M} l_m S_{j-1,((2j-m) \bmod N/2^{j-1})+1} \quad (4)$$

where h and l are high-pass and low-pass filters, respectively. $f_{j,t}$ and $F_{j,t}$ are detail and approximation coefficients at level j, respectively.

Reconstruction to the original signal can be performed by the detail coefficient and approximate coefficient, and repeating this

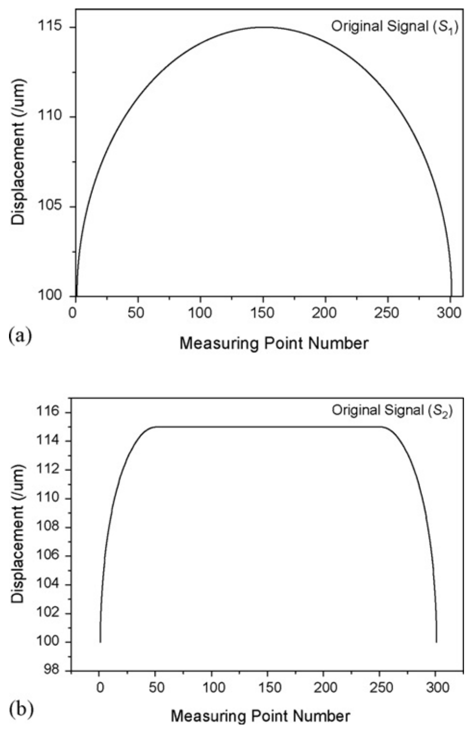

Fig. 8. The theoretical simulated signals. (a) The theoretical signal of sensor 1. (b) The theoretical signal of sensor 2.

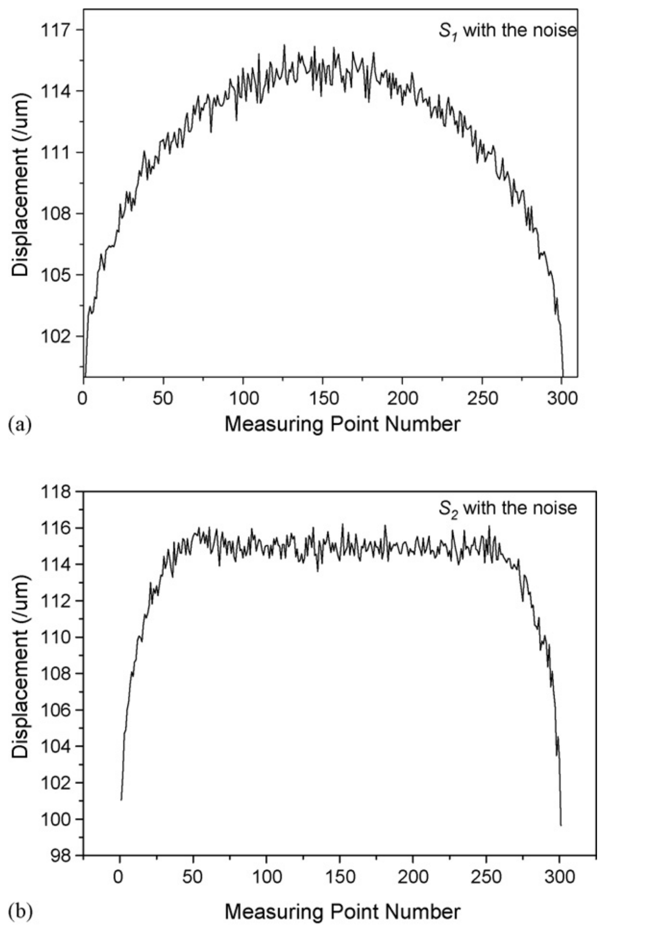

Fig. 9. The simulated signals with the noise. (a) The noisy signal of sensor 1. (b) The noisy signal of sensor 2.

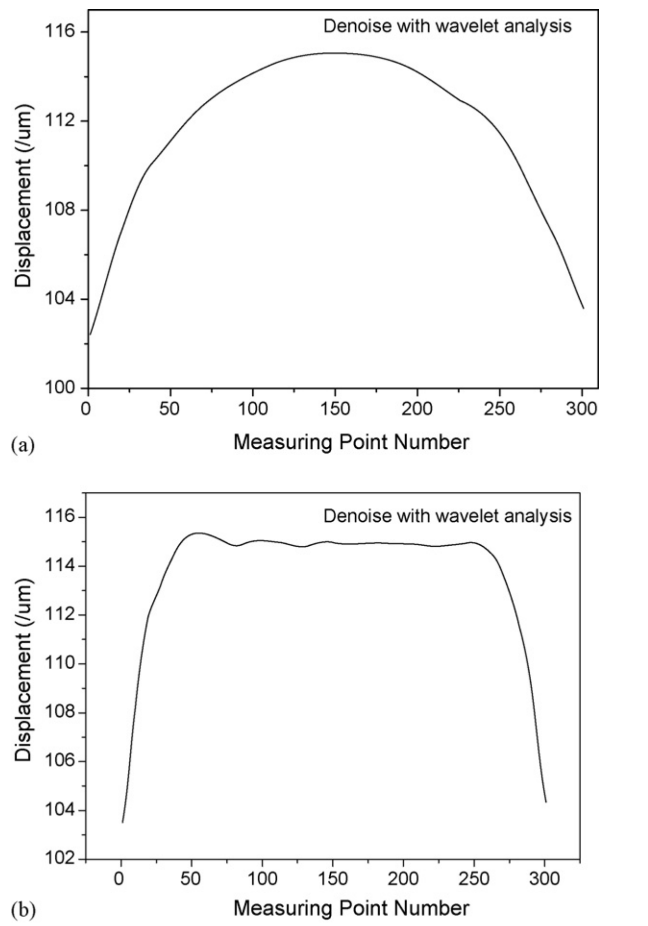

Fig. 10. The purified signals in the simulation experiment with wavelet analysis. (a) The purified signal of sensor 1. (b) The purified signal of sensor 2.

process finally gives an original signal as $S_{0,t}$:

$$S_{j,t} = \sum_{m=1}^{M} h_m f^0_{j+1,((t+m-2)\bmod N/2^j)+1} + \sum_{m=1}^{M} l_m F^0_{j+1,((t+m-2)\bmod N/2^j)+1} \tag{5}$$

3.3. Simulation experiments

The simulation experiments show that FFT filter and wavelet analysis can be used to denoise from the practical data and the wavelet method is prior to FFT in the noise removal of the practical data. Fig. 8 shows the theoretical original signals: (a) is sensor 1 and (b) is sensor 2. The signal of sensor 1 is an arc and sensor 2 is a constant. The flange thickness can be obtained by the maximum value of (a) and the value of (b) correspondingly. The original signals are contaminated with additive the noise. The noise is the random function of the normal distribution and obtained with Matlab function defined according to Eq. (6).

$$\text{noise} = 0.5\,\text{randn}(1, \text{count1}) \tag{6}$$

The noisy signals are shown in Fig. 9. The maximum value of (a) and the value of (b) correspondingly are masked by the noise and can hardly be found.

Firstly the FFT method is used to remove the noise. It is noted that FFT seems to give good results, but the FFT smoothing method heavily distorts the signal.

The second method used to denoise is the wavelet analysis. Different families of wavelets are compared and the results show that the choice of the wavelet family plays an important role in the denoising of the signals. The sym wavelet family (Sym5) and 5-level

Table 1
System's original results, and wavelet reconstruction results, and manual measuring results (unit: mm).

Wheelset number	Left wheel			Right wheel		
	Manual measure	System measure		Manual measure	System measure	
		Original	Wavelet		Original	Wavelet
1	32.3	31.7	32.2	32.3	32	32.1
2	31.7	31.4	31.8	32.7	31.9	32.5
3	31.8	31.8	32	32.6	31.7	32.1
4	32.1	31.2	31.8	32.3	31.4	32.3
5	31.9	31.8	32	32.6	32.3	32.4
Mean value	31.96	31.58	31.96	32.5	31.86	32.28
RMSE	0.22	0.24	0.18	0.19	0.30	0.18

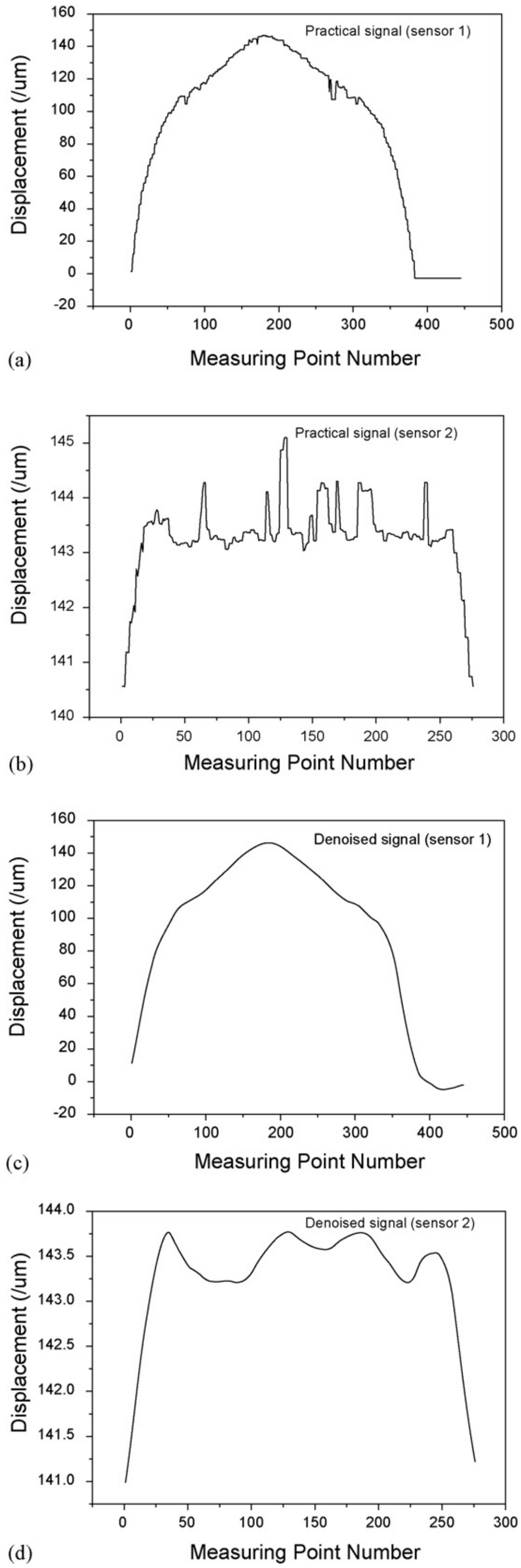

Fig. 11. The practical and denoised signals of sensor 1 and sensor 2 with the wavelet analysis. (a) The practical signal of sensor 1. (b) The practical signal of sensor 2. (c) The denoised signal of sensor 1. (d) The denoised signal of sensor 2.

decomposition are the best for the detecting signals of the sensor 1 and sensor 2. Fig. 10 shows the reconstruction signals with the wavelet analysis: (a) is the purified signal of sensor 1 and (b) is the purified signal of sensor 2.

4. Measurement results and discussion

Fig. 11 shows the practical and denoised signals of sensor 1 and sensor 2 with the wavelet analysis: (a) is the practical signal of sensor 1, and (b) is the practical signal of sensor 2, and (c) is the denoised signal of sensor 1 with the wavelet analysis, and (d) is the denoised signal of sensor 2 with the wavelet analysis.

Table 1 shows that the multiple measuring results of the system when wheelsets pass through it at the speed of 10 km/h. The results will be varied at different detecting position because of the wheelset creeping. The experimental results are compared to the manual measuring results to verify the measuring accuracy and reliability. 5 times measurements are accomplished by the operators and by the system respectively. The manual measurements are obtained by the gauge whose precision is 0.2 mm. The root-mean-square errors (RMSE) of the left wheels of the manual measurement, and the original measurement, and the wavelet analysis are 0.22, and 0.24, and 0.18 respectively. The changing range of manual measurement is much larger than the system because of the difference between every operator's measuring standard. That shows the system has the better repeatability and reliability. These results show that the system based on the laser displacement sensors can meet with the measuring requirement on line.

5. Conclusions

The flange thickness is key parameter that influences the wheel–rail contact. The measuring system based on the laser displacement sensors is proposed to measure this parameter on line. The measuring results are improved by the wavelet analysis. The RMSE of the left wheels of the manual measurement, and the original measurement, and the wavelet analysis are 0.22, and 0.24, and 0.18 respectively. The changing range of manual measurement is much larger than the measuring system because of the difference between every operator's measuring standard. That shows the measuring system has the better repeatability and reliability. These results show that the system based on the laser displacement sensors can meet with the measuring requirement on line.

Acknowledgement

This research work is supported by Doctor's Innovation Fund of Zhengzhou University of Light Industry.

References

[1] B. Francisco, B. Stefano, R. Ferruccio, Wear of railway wheel profiles: a comparison between experimental results and mathematical model, Vehicle Syst. Dyn. 37 (Suppl.) (2003) 478.
[2] K. Hiromichi, F. Takehiko, Measuring rail/wheel contact points of running railway vehicles, Wear (253) (2002) 275–283.
[3] Joes Luis Lopez Gomez. Installation for measuring the wheel offset of railway vehicles. US6003232.
[4] Danneskiold-Samsoe. Apparatus for track-based detection of the wheel profile of passing railway wheels. US4932784.
[5] Mian. Contactless wheel measurement system and method. US006768551B2.
[6] X. Gao, N. Wu, G. Li, et al., A new device for automatically detecting wheelset parameters of railway vehicles, New Technol. New Process 2 (2003) 9–11.
[7] Y.-h. Ao, G.-h. Li, N.-y. Wu, Application of sensors in measuring system for train wheel parameter, J. Transducer Technol. 22 (6) (2003) 39–41.
[8] Photoelectric measurement for geometrical parameters and tread defects of wheel set, Opto-Electron. Eng. 32 (7) (2005) 48–51.
[9] J.-y. Zuo, W.-x. Zhou, J. Zeng, et al., Test and research on measurement of wheel rim dimensions with laser sensor, Railway Vehicle 40 (2) (2002) 11–13.

[10] F.-f. Zheng, J. Liu, P.-x. Fan, Research on measuring shape of wheel set treads with the digital camera, Railway Vehicle 40 (1) (2002) 19–22.
[11] C. Yuri, P. Sergei, P. Anatoly, V. Alexander, Novel optical measuring systems and laser technologies for science and industry, in: Third International Symposium On precision Mechanical Measurements, SPIE, no. 3, 2006, pp. 1–10.
[12] S.G. Newton, et al., An investigation into the dynamic errors on the track or wheel flats on railway vehicles, J. Mech. Eng. Sci. (4) (1979) 287–297.
[13] K. Wu, J. Zhang, K. Yan, Online measuring method of the wheel set wear based on CCD and image processing, Adv. Mater. Devices Sensing Image, SPIE 5633 (2005) 409–415.
[14] Sumit K. Nath, R.M. Vasu, M. Pandit, Wavelet based compression and denoising of optical tomography data, Opt. Commun. 167 (1999) 37–46.
[15] B.J. Woodford, D. Deng, G.L. Benwell, A wavelet-based neuro-fuzzy system for data mining small image sets, ACM Int. Conf. Proc. Ser. 32 (2004) 139–143.
[16] Q. Duan, E. Angelini, T. Song, A. Laine, Fast interpolation algorithms for three-dimensional real-time cardiac ultrasound, in: Proceedings of the 25th Annual international Conference of the IEEE, vol. 2, 2003, pp. 1192–1195.
[17] J.P. Martinez, R. Almeida, S. Olmos, A.P. Rocha, P. Laguna, A wavelet-based ECG delineator: evaluation on standard databases, Biomed. Eng. IEEE Trans. 51 (2004) 570–581.
[18] B. Olshausen, in: L.M. Chalupa, J.S. Werner (Eds.), The Visual Neurosciences, MIT Press, Cambridge, MA, 2003, pp. 1603–1615.
[19] M. Fligge, S.K. Solanki, Noise reduction in astronomical spectra using wavelet packets, Astron. Astrophys. Suppl. Ser. 124 (1997) 579–587.
[20] M. Fligge, S.K. Solanki, Noise reduction in astronomical spectra: a new wavelet-based method, Cool Stars Stellar Syst. Sun ASP Conf. Ser. 154 (1998) 833–837.
[21] J. Portilla, E.P. Simoncelli, A parametric texture model based on joint statistics of complex wavelet coefficients, Int. J. Comput. Vis. 40 (1) (2000) 49–71.
[22] A.V. Oppenheim, A.S. Willsky, S. Hamid Nawab, Signals & Systems, 2nd ed., Prentice-Hall, Inc., 1996.
[23] Q. Zhang, R. Aliaga-Rossel, P. Choi, Denoising of gamma-ray signals by interval-dependent thresholds of wavelet analysis, Meas. Sci. Technol. 17 (2006) 731–735.